Structural characterization of nanoparticles formed by fluorinated poly(2-oxazoline)-based polyphiles

Anna Riabtseva, Leonid Kaberov, Laurence Noirez, Vasyl Ryukhtin, Corinne Nardin, Bart Veerbraeken, Richard Hoogenboom, Petr Stepanek, Sergey Filippov

Structural characterization of nanoparticles formed by fluorinated poly(2oxazoline)-based polyphiles

Anna Riabtseva[a], Leonid I. Kaberov[a], Laurence Noirez[b], Vasyl Ryukhtin[c], Corinne Nardin[d], Bart Verbraeken[e], Richard Hoogenboom[e], Petr Stepanek[a], Sergey K. Filippov[a,*]

[a] Institute of Macromolecular Chemistry, Academy of Sciences of the Czech Republic, Heyrovský Sq. 2, 162 06 Prague 6, Czech Republic [b] Laboratoire Léon Brillouin (CEA-CNRS), UMR12, Université Paris-Saclay, CEA-Saclay, F-91191 Gif-sur-Yvette, France [c] Nuclear Physics Institute, ASCR, v.v.i., Husinec-Řež 250 68, Czech Republic

[d] Université de Pau et des Pays de l'Adour/CNRS, Institut des Sciences Analytiques et de Physico-chimie pour l'Environnement et les Matériaux, UMR5254, 64000 Pau, France

[e] Supramolecular Chemistry Group, Department of Organic and Macromolecular Chemistry, Ghent University, Krijgslaan 281 S4, B-9000 Ghent, Belgium

A B S T R A C T

We report on the self-assembly behavior of poly(2-methyl-2-oxazoline)–block–poly(2-octyl-2-oxazoline) comprising different terminal perfluoroalkyl fragments in aqueous solutions. As reported previously [Kaberov et al. (2017)] such polyphiles can form a plethora of nanostructures depending of the composition and on the way of preparation. Here we report, for the first time, detailed information on the internal structure of the nanoparticles resulting from the self-assembly of these copolymers. Small-angle neutron and X-ray scattering (SANS/SAXS) experiments unambiguously prove the existence of polymersomes, wormlike micelles and their aggregates in aqueous solution. It is shown that increasing content of fluorine in the poly(2-oxazoline) copolymers results in a morphological transition from bilayered or multi-layered vesicles to wormlike micelles for solutions prepared by direct dissolution.

In contrast, nanoparticles prepared by dialysis of a polymer solution in a non-selective organic solvent against water are characterized by SAXS method. The internal structure of the nanoparticles could be assessed by fitting of the scattering data, revealing complex core-double shell architecture of spherical symmetry. Additionally, long range ordering is identified for all studied nanoparticles due to the crystallization of the poly(2-octyl-2oxazoline) segments inside the nanoparticles.

1. Introduction

Owing to their versatile properties, poly(2-alkyl/aryl-2-oxazoline)s (PAOx) and their derivatives currently receiving significant scientific attention [1–3]. Due to their biocompatibility and nontoxicity, PAOx are widely studied as materials for biomedical applications such as drug, protein, radionuclide or gene delivery [4–7] as well as for the preparation of non-fouling surfaces that resist non-specific adsorption of proteins, bacteria, and higher organisms [8]. Living cationic ringopening polymerization (CROP) is usually used for the synthesis of polyoxazolines [9,10] and allows not only controlling the molecular weight and dispersity of the resulting polymers but also to obtain PAOx of desired architecture. One can vary the nature and ratio of monomers, use different functional initiators or terminate agents thereby introducing fragments with different functionality and controlling the hydrophilic to hydrophobic balance [11–13].

Varying the ratio and the order of hydrophilic and hydrophobic blocks constituents of amphiphilic PAOx leads to a plethora of self-assembled structures such as spheres [14], vesicles [15], rod- or wormlike micelles, cylinders and corresponding aggregates in solution. Usually, poly(2-methyl-2-oxazoline) (MeOx) or poly(2-ethyl-2-oxazoline) (EtOx) are used to build hydrophilic blocks since these are biocompatible and reveal “stealth-like” behavior [16–18]. More complex structures, for example, multicompartment micelles, could be obtained upon self-assembly of triblock terpolymers in water or organic solvents [19,20]. Especially interesting are the so-called polyphiles - triblock copolymers that combine hydrophilic, hydrophobic and fluorophilic blocks [21–25]. Due to the immiscibility of the lipophilic and fluorophilic hydrophobic segments the resulting copolymers can form particles of complex morphologies depending on the polymer architecture and solvent [20,26,27]. Such nano- and microparticles containing fluorinated fragments are of high interest for potential application as magnetic resonance imaging contrast agents [28,29].

* Corresponding author.
E-mail address: filippov@imc.cas.cz (S.K. Filippov).

https://doi.org/10.1016/j.eurpolymj.2018.01.007
Received 26 November 2017; Received in revised form 3 January 2018; Accepted 10 January 2018 Available online 11 January 2018
0014-3057/

While the synthesis and the self-assembly behavior of di- and triblock PAOx containing hydrophilic and hydrophobic blocks were widely studied, there is not much information about triblock PAOx that contain fluorinated moieties. Schubert and co-authors reported on the investigation of nanostructures formed by triblock terpolymers consisting of poly[2-ethyl-2-oxazoline-block-2-(1-ethylpentyl)-2-oxazolineblock-2-(Xfluorophenyl)-2-oxazoline] (X =di, tri, tetra and penta). The authors studied the influence of the fluorination degree of these polymers on their self-assembly ability. A transition from rod-like micelles to highly complex round-shaped super-aggregates was observed by cryo-TEM with

increasing fluorine content [30]. Water-soluble polymer surfactants based on 2-methyl-2-oxazoline with both fluorinated terminal group $C_8H_{17}CH_2CH_2$ (constant length) and hydrocarbon terminal group of different lengths C_nH_{2n+1} (n = 6,8,…,18) were synthesized by Nuyken and co-authors [31]. It was shown by the fluorescence spectroscopy of polymer solutions with solubilized pyrene that micelle core composition and first micellization point depends on the ratio between hydrophobic and fluorocarbon parts of polymer.

Recently we reported on the synthesis and solution properties of a novel quasi-triblock fluorine-containing copolymers based on 2-oxazolines [32]. Our synthetic approach provides an easy way to attach a

C_nF_{2n+1} perfluorinated terminal chain to a poly(2-methyl-2-oxazoline)–block–poly(2-octyl-2-oxazoline) (PMeOx-b-POctOx) dilock copolymer through termination and to combine hydrophilic, hydrophobic and fluorophilic moieties along one polymer chain. Preliminary investigations of the self-assembly of the synthesized polymers in water using dynamic light scattering and cryo-TEM revealed the coexistence of bilayer and multi-layer vesicles as well as rod-like micelles. The shape and the size of the nanoparticles in solution could be controlled by the way of preparation. Spherical micelles with diameters ranging from 15 to 20 nm were observed in solution for the polymers assembled by solvent exchange. However, more detailed insights into the internal structure (size of the core and the shell thickness) of the formed nanoparticles and their dependence on the length of the fluorinated fragment or the method of preparation were not investigated.

Here, we report on the in depth evaluation of the internal structure of nanoparticles formed by the self-assembly of quasi-triblock fluorinecontaining copolymers, namely PMeOx-POctOx-C_8F_{17}, PMeOx-POctOx$C_{10}F_{21}$, PMeOx-POctOx-$C_{12}F_{25}$, as well as the non-fluorinated PMeOx-bPOctOx reference diblock copolymer. We describe the influence of the length of the perfluorinated terminal chain and of the preparation methods on the features of the self-assembled polymers. To achieve a comprehensive characterization of the morphology of the resulting nanoparticles, we combined both small-angle X-ray scattering (SAXS) and small-angle neutron scattering (SANS) experiments.

2. Experimental section

2.1. Materials

2-Methyl-2-oxazoline (MeOx, 99%, Acros Organics) was dried over BaO and distilled before use. 2-(n-octyl)-2-oxazoline (OctOx) was synthesized according to procedure described elsewhere [32]. Perfluorinated acids (nonanoic, undecanoic, tridecanoic) and p-toluenesulfonate were purchased from Sigma-Aldrich and used as received. Acetonitrile (ACN, Lachner) was dried by refluxing over BaO and distilled before use. Water was deionized with a MilliPore Milli-Q® gradient installation. All other chemicals were used as received.

2.2. Polymer synthesis

All copolymers were synthesized separately by the CROP. The detailed procedure was described in our previous work [32]. In brief, the first monomer MeOx and the initiator (p-toluenesulfonate) were dissolved in acetonitrile and stirred at 140 °C in pressure reactor under

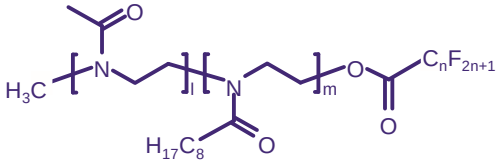

Scheme 1. Chemical structure of quasi-triblock copolymers, n =8, 10 or 12.

Table 1
Composition and characteristics of fluorinated quasi-triblock poly(2-oxazolines) and reference nonfluorinated diblock copolymer.

Polymer	Composition	M_n, g/mol	Đ
P0	$PMeOx_{30}$-b-$POctOx_{20}$	6300	1.11
P1	$PMeOx_{30}$-b-$POctOx_{20}$-C_8F_{17}	6000	1.08
P2	$PMeOx_{30}$-b-$POctOx_{20}$-$C_{10}F_{21}$	5000	1.09
P3	$PMeOx_{30}$-b-$POctOx_{20}$-$C_{12}F_{25}$	5000	1.14

inert atmosphere for 35 min (≈98% of conversion). After cooling down the reaction mixture, the second monomer OctOx was added and the mixture was stirred at 140 °C for another 45 min to form diblock copolymer.

The perfluoroalkyl fragments were attached to copolymers by termination of polymerization with corresponding perfluorinated carboxylic acids in the presence of triethylamine at 70 °C. To obtain the model PMeOx-b-POctOx diblock copolymer, the polymerization was quenched with 1 M KOH in methanol.

The chemical structures of the polymers are shown in Scheme 1. The molecular weights of the polymers range from 5 to 6 kDa, and the polydispersities of the samples according to the reference [32] in range from 1.08 to 1.14 (Table 1).

2.3. Preparation of samples

All solutions for SAXS experiments were prepared using deionized water in the range of concentrations from 0.1 to 5 wt%. All solutions for SANS experiments were prepared using D_2O (99.9%, Sigma-Aldrich) as solvent to reduce the incoherent scattering. The concentration of all SANS solutions was 2 wt%. Scattering from pure H_2O or D_2O was measured separately and subtracted from solution scattering data.

Samples for SAXS and SANS experiments were prepared in two ways: by direct dissolution in H_2O or D_2O or by solvent exchange.

2.3.1. Solvent exchange method

Briefly, 5 mL of 2.5 wt% polymer solution in methanol was placed in dialysis tubing with MWCO 3.5–5 kDa (Spectra/Por, Spectrum Laboratories, Inc.) and dialyzed against 5 L of deionized water with mild stirring at 25 °C. The deionized water was refreshed 5 times and the total dialysis time was 24 h. Samples were stored in sealed containers at 4 °C.

2.4. Small-angle X-ray scattering

SAXS experiments for samples prepared by direct dissolution were performed on the high brilliance beamline ID02 at ESRF (Grenoble, France). The SAXS setup utilizes a pinhole camera with a beam stop placed in front of a two-dimensional Frelon CCD detector. The X-ray scattering patterns were recorded for sample-to-detector distances of 2.5 and 31 m, using a monochromatic incident X- ray beam with an energy of E =12 460 eV (λ =0.1 nm). The available scattering vector range was q = 0.001–2.76 nm^{-1} ($q = 4\pi \sin\theta/\lambda$, where 2θ is the scattering angle). Online corrections were applied for the detector, and the sample-to-detector distance, center, transmission, and incident intensity were

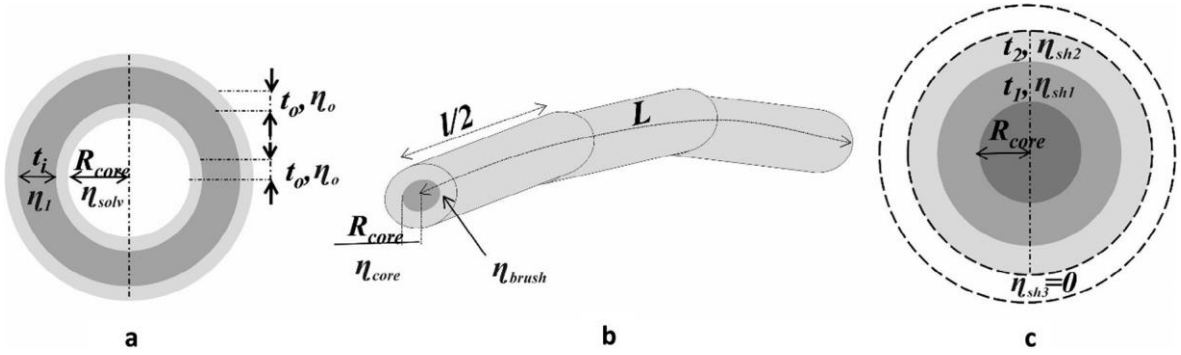

Fig. 1. Scheme of bilayered vesicle (a), wormlike micelle (b) and sphere with three shells (c).

calibrated. The isotropic scattering was azimuthally regrouped to determine the dependence of the scattered intensity I(q) on the scattering vector q in absolute units. The scattering from a capillary filled with Milli-Q water was measured as a background and subtracted from the scattering signals of the samples. Prior to the experiment, a representative sample was checked to ensure lack of radiation damage.

SAXS experiments for samples obtained through solvent exchange from methanol were performed at the beamline B21 (Diamond Light Source, Didcot, UK) using a pixel detector (2M PILATUS). The X-ray scattering images were recorded for a sample-to-detector distance of 3.9 m, using a monochromatic incident X-ray beam (λ =0.1 nm) covering the range of scattering vector 0.025 nm^{-1} < q < 4 nm^{-1}. Most of the samples had no measurable radiation damage by the comparison of 20 successive time frames with 50 ms exposures. The two-dimensional scattering patterns were

azimuthally averaged to yield the dependence of the scattered intensity I(q) on the scattering vector q. Before fitting analysis, the solvent scattering has been subtracted.

2.5. Small-angle neutron scattering

SANS experiments for samples prepared by direct dissolution were performed at CEA-Saclay on the spectrometer PAXY of the Laboratoire Leon-Brillouin. Measurements were performed with a 128 ×128 multidetector (pixel size 0.5 ×0.5 cm) using a monochromatic (wavelength λ set by a mechanical velocity selector) incident neutron beam collimated with circular apertures for two sample-to-detector distances, namely, 1 m (with λ =0.6 nm) and 7 m (with λ=0.8 nm). With such a setup, the investigated range of scattering vector is from 5×10^{-2} to 4×10^{-1} nm^{-1}. The two-dimensional scattering patterns were isotropic so that they were azimuthally averaged to yield the dependence of the scattered intensity I(q) on the scattering vector q.

3. Data analysis

The SANS and SAXS data were fitted using several models implemented in the SASfit software [33] (http://kur.web.psi.ch/sans1/ SANSSoft/sasfit.html). The curves were fitted using the following function:

$$I(q) = P(q)\, S_{HS}(q) + P_{Voigt}(q) + I_{bkg} \qquad (1)$$

where P(q) is the form factor of the scattering object, $S_{HS}(q)$ is the structure factor for hard sphere interaction (Percus–Yevick model), $P_{Voigt}(q)$ is Voigt peak form factor, which describes peaks in the high q range of scattering curves and I_{bkg} is the incoherent background.

Scattering length densities (SLDs) of polymeric parts for all implemented models (Tables S2 and S3) were freely fitted during the fitting procedure and compared to estimated values of SLD to decide whether the fit results were in agreement with theoretical ones (Table S1). SLD of D_2O and H_2O were fixed to the literature values of
6.33×10^{-4} nm^{-2} and 9.44×10^{-4} nm^{-2}, respectively.

3.1. Structure factor

To take into account the interactions between nanoparticles we used Perkus-Yevick structure factor for hard spheres $S_{HS}(q)$ [34]:

$$S_{HS}(q) = \frac{1}{1 + 24 f_{HS}\, G(2R_{HS}q)/(2R_{HS}q)}$$

where R_{HS} is radius of hard sphere and f_{HS} is hard-sphere volume fraction. The function G(x) is given by:

$$\sin x - \cos x 2x \sin x + (2 - x^2)\cos x - 2$$

$$G(x = \gamma' \frac{}{x^2} + \delta' \frac{}{x^3} + \varepsilon' \frac{-x^4 \cos x + 4(3x^2 - 6\cos x + (x^3 - 6x \sin x + 6)}{x^5}$$

where $\gamma' = \frac{(1+2f_{HS})^2}{(1-f_{HS})^4}$, $\delta' = \frac{-6f_{HS}(1+f_{HS}/2)^2}{(1-f_{HS})^4}$, $\varepsilon' = \frac{\gamma' f_{HS}}{2}$

3.2. Bilayered vesicle

The form factor of bilayered vesicle $P_{BLV}(q)$ was used for diblock copolymer $PMeOx_{30}$-b-$POctOx_{20}$ and as one of the possible form factors for triblock copolymer with the shortest perfluorinated fragment $PMeOx_{30}$-b-$POctOx_{20}$-b-C_8H_{17}:

$$PBLV(\ )q = (K\ q\ R(\ , core, \eta solv - \eta i) + K\ q\ R(\ , core + t\ \eta o, i - \eta o) + K\ q\ R(\ , core + ti + t\ \eta o, o - \eta i) + K\ q\ R(\ , core + 2ti + t\ \eta o, i - \eta solv))2 \quad (2)$$

with

$$\frac{4}{3}{}^3\Delta\ 3\eta\ \sin qR\ qR - \cos qR\ K\ (q\ R, ,\Delta\eta) = \pi R \quad (3)$$

where R_{core} is the radius of bilayered vesicles core, which consists of solvent, t_o is thickness of outer part of bilayer, t_i is thickness of inner part of bilayer. η_o, η_i, η_{solv}, are SLD of outer part of bilayer, inner part of bilayer and solvent, respectively. The scheme of bilayered vesicle model is shown on the Fig. 1a. To account for polydispersity, a Schulz-Zimm distribution of R_{core} was included.

For solutions with concentration below 1% no structure factor was needed and $S_{HS}(q)$ was set to 1.

3.3. Wormlike micelle

The overall scattering intensity of wormlike micelle with contour length L and Kuhn length l can be written as [35]

$$Pwm = Nagg2\ \beta core2\ Pcore(\ )q + Nagg\beta brush2Pbrush(\ )q + 2Nagg2\ \beta core\beta brushSbrush - core(q) + Nagg\ (Nagg - 1)\beta_{brush}{}^2 Sbrush - brush(\ )q\ ,$$

where $N_{agg}{}^2\ \beta_{core}{}^2\ P_{core}(q)$ is self-correlation term of the core, $N_{agg}\beta_{brush}{}^2\ P_{brush}(\ )q$ is self-correlation term of the chains,

$2N_{agg}{}^2\ \beta_{core}\beta_{brush}S_{brush-core}(q)$ is the cross-term between the core and chains and $Nagg\ (Nagg - 1)\beta brush2\ Sbrush - brush(\ )q$ is the cross-term between different chains. N_{agg} is the aggregation number of polymers forming the micelle per surface area, $\beta brush = Vbrush\ (\eta brush - \eta solv)$ and $\beta core = Vcore\ (\eta core - \eta solv)$ are the excess scattering lengths of a block in the corona and in the core, respectively. V_{brush} and V_{core} are the total volume of a block in the corona and in the core, respectively. η_{brush} and η_{core} are the corresponding SLDs. $P_{core}(\ )q$ is scattering of wormlike core and can be written

as the product of the scattering from the conformation of worm $P_{worm}(q\ l\ L,\ ,\ )$ and the cross section scattering $P_{cs}(q\ R,\ _{core},\ ,d\ R_g)$

$$Pcore\ (q\ R,\ core,\ ,\ )l\ L = Pworm\ (q\ l\ L\ P,\ ,\ )\ cs\ (q\ R,\ core,\ ,d\ Rg)$$

,where R_{core} is radius of wormlike core with uniform scattering length density

$$R_{core} = \sqrt{\frac{N_{agg}V_{core}}{1-x_{solv\ core},}\cdot\frac{1}{\pi L}}$$

where $x_{solv\ cor,e}$ is amount of solvent in the micellar core.

The contribution of wormlike conformation P_{worm} is described by the model from Kholodenkos approach [36]

$$P_{worm}(q\ l\ L,\ ,\ ) = I\ x_2(\ )], \text{ where } x = \frac{\frac{2l}{3L}[I_1(\ )-\frac{l}{3L}}{\underline{3L}}$$

$$I\ x_n(\ ) = \int_0^{l\ x} f\ z\ z(\ )^{n-1}dz$$

$$\begin{cases} \left|\underline{E}_{\sinh} z\ for q \leqslant l\ f(\ )z = {}_1\sinh(Fz)\ 3\ , \right. \\ \left.\underline{for q} > \left|\underline{F}\sinh z \right.\right. \end{cases}$$

$$\sqrt{\ } \quad {}_2\ 2\sqrt{\text{where } E = \ 1-(\ )^{lq}} \text{ and } F = (\ )^{lq} \quad -1.$$

$${}_3\ 3$$

For the contribution of the cross section P_{cs} is given as

$$\overline{\quad} \quad 2\ Pcs\ (q\ R,\ core,\ ,d\ Rg) = \left[\left|\left[2J\ qR1qR(\ _{core}core)\right]\right|\right],$$

where R_g is radius of gyration of the block unit in the corona, J_1 is the first order Bessel function of the first kind: $J(\ )x = (\sin x - x\cos\ )/x \quad x^2$.

The scattering intensity for the brush of wormlike micelle is given by:

$$Pbrush\ (q\ R,\ g) = \frac{exp(-\ -\ +x)\ 1 \quad x}{x^2}{}_2 \quad ,$$

where $x = R\ q_g{}^2 \quad {}^2$.

The contribution of cross term between core and chains which form brush of wormlike micelle is calculated using equation:

$2J\ qR1(\quad core)$

$Sbrush{-}core\ (q\ R,\ core,\ ,\ ,l\ L\ R\ dg,\ ) = \psi\ qR(g)$ ______ $J\ q\ R0\ [\ (\ core$

qR_{core}

$+\ dR_g)]P_{worm}\ (q\ l\ L,\ ,\ )$

The contribution of cross term between chains is calculated using equation:

$Sbrush{-}brush\ (q\ R,\ core,\ ,\ ,l\ L\ R\ dg,\ ) = \psi 2\ (qR\ Jg)\ 02\ [\ (q\ Rcore + dRg)]Pworm\ (q\ l\ L,\ ,\ )$, where $\psi(qR_g) =$ ______ $^{1-exp}{}_x{}^{(-x)}$ is the form factor amplitude of the chain, J_0 is the zeroth order Bessel function of the first kind, d is parameter that accounts non-penetration of the chains into the core and should be mimicked by $d{\sim}1$ for $R_{core} \gg R_g$.

To account for polydispersity, a Schulz-Zimm distribution of R_g was included. The structure factor S(q) in the case of fitting with wormlike micelles model was set to 1. The model of wormlike micelle is presented on the Fig. 1b.

3.4. Sphere with three shells

The SAXS data obtained for dialyzed samples were fitted with a model 'Sphere with 3 shells' implemented in the SASFit software (Fig. 1c). To utilize this model for fitting SAXS curves of studied polymers the thickness of the third shell was set as 0 and its SLD was the same as SLD of H_2O. The scattering intensity for sphere with 3 shells, $P_{S\ Shell3}\ (q)$, is calculated based on the core-shell model [37] and is given by:

$PS\ Shell3(\ )q = (K\ q\ R(\ ,\ core,\eta core{-}\eta sh1) + K\ q\ R(\ ,\ c + t\ \eta 1,\ sh2{-}\eta sh1)$

$+\ K\ q\ R(\ ,\ core + t1 + t\ \eta 2,\ sh3{-}\eta sh2) + K\ q\ R(\ ,\ core + t1 + t2 + t\ \eta 3,\ sh3$

$-\eta solv))2$

were $K\ (q\ R,\ ,\Delta\eta)$ is calculated using Eq. (2), t_1, t_2, t_3 are thicknesses of the first, second and third shell, η_{core}, η_{sh1}, η_{sh2}, η_{sh3} are SLDs of core and shells, respectively.To account for polydispersity, a Schulz-Zimm distribution of R_{core} was included.

3.5. Voigt peak

Voigt function was used to describe the shape of the peaks at high q range of scattering curves. The amplitude version of the Voigt peak is parameterized as

$\int^{\infty} \frac{exp(-u^2)}{2}\ {}_2 du$

$-\infty\ 2\gamma\sigma\ \ x\ x{-}2\sigma^c \qquad \frac{u}{}\ \ V\ x\ x\ \sigma\ \gamma(\ ,\ {}_c|\ ,\ )$

$VAmplitude\ (x\ A\ \sigma\ \gamma|\ ,\ ,\ ) = A \quad 2 \quad = A$

$\int_{-\infty}^{\infty} \frac{exp(-u\ )}{2} du \quad V\ x\ x\ \sigma\ \gamma(\ {}_c,\ {}_c|\ ,\ )$

$\frac{\gamma}{2\sigma^2} + u$

where A is an amplitude of the Voigt peak, x_c is location parameter, σ is width of Doppler contribution, γ is a width of Lorentzian contribution. The modified Porod function was used to describe the contribution of large aggregates at the lowest q range: $C_0 + {}_q{}^c{}_\alpha{}^1$, where α is modified Porod exponent.

4. Results and discussion

4.1. Nanoparticles prepared by direct dissolution

The SANS and SAXS curves of all the copolymers at a concentration of 2 wt% and 2.5 wt%, respectively, are presented in Fig. 2a and b.

For the reference $PMeOx_{30}$-b-$POctOx_{20}$ diblock copolymer at low q range the scattering intensity follow a power law of $I \sim q^{-2.53 \pm 0.02}$ for SANS and $q^{-2.25 \pm 0.01}$ for SAXS (Fig. 3a and b). Such scaling exponent implies planar like structure. In the middle q range, the scattered intensity is decreasing and obeys a power law of $I \sim q^{-4.38 \pm 0.08}$ that corresponds to the scattering of compact structures with a sharp interface. The SANS and SAXS data were quantitatively analyzed by fitting the scattering curves with an appropriate model as shown in Fig. 1.

The fitting parameters are presented in Table 2 and explained above in Data analysis section.

The scattering data corresponding to the structures of the self-assembled diblock copolymer can be fitted using the bilayered vesicle form factor corrected with the Schultz–Zimm polydispersity over R_a. These findings are in agreement with previously reported cryo-TEM imaging of diblock copolymer $PMeOx_{30}$-b-$POctOx_{20}$, where bilayered vesicles were revealed [32]. Additionally, the contribution of large aggregates was added as background, which resulted in a good quality fit. The quantitative analysis of the SANS scattering data yields a radius of vesicle interior, R_a, consisting of solvent of 24.4 nm and a polydispersity value of 0.26. The hydrophobic layer, t_i, consists of presumably the POctOx block of 1.6 nm thickness, whereas the hydrophilic PMeOx layer thickness, t_h, is 2.48 nm. The total radius of the vesicle is approximately 28.5 nm according to the SANS data. These values are in agreement with Cryo-TEM images where polydispersed vesicles in the

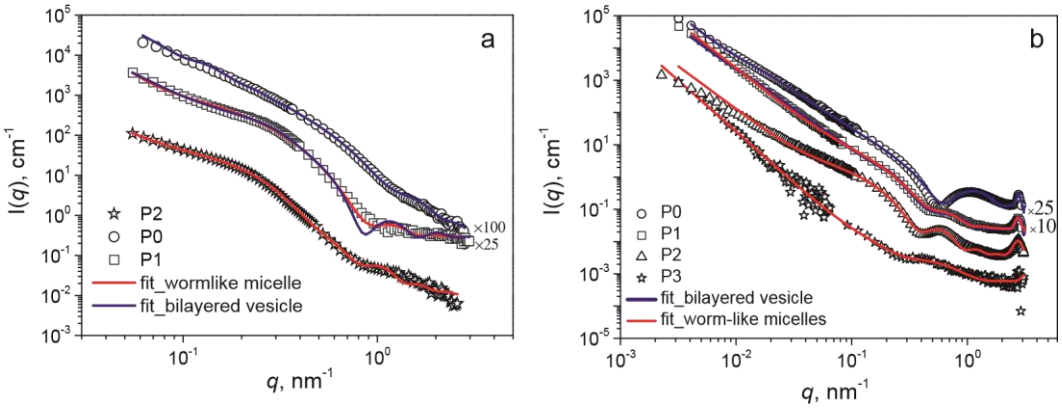

Fig. 2. SANS (a) and SAXS (b) curves displayed by $PMeOx_{30}$-b-$POctOx_{20}$ (P0), $PMeOx_{30}$-b-$POctOx_{20}$-C_8F_{17} (P1), $PMeOx_{30}$-b-$POctOx_{20}$-$C_{10}F_{21}$ (P2) and $PMeOx_{30}$-b-$POctOx_{20}$-$C_{12}F_{25}$ (P3) aqueous solutions prepared by direct dissolution.

range 20–50 nm are observed.

A similar scattering pattern was obtained by the SAXS measurements (Fig. 3b). However, the SAXS scattered intensity has a broad secondary maximum in the q-range from 0.7 to 2 nm^{-1}, that can be explained by the differences in SLD values of the inner and outer bilayer parts on the solvent side. Such phenomenon was experimentally observed in a variety of other reported studies [38,39]. Values of the bilayer and outer layer thickness are in rather good agreement with those calculated from SANS data (Table 2). At the highest q value, the scattering curves for higher concentrations of aqueous diblock copolymer solutions exhibit another peak located at q = 2.75 nm^{-1} (Fig. 4a (inset)).

We utilized the bilayered vesicle model with Schultz −Zimm polydispersity and contribution from aggregates and in order to describe the small sharp peak at high q values the Voigt peak model was used (Ref. [40]), which can be attributed to additional internal ordering. From the position of the peak the repeat distance can be calculated as $D = 2\pi/q$, being 2.27 nm (Table 2). This ordering can be explained by the crystallization of octyl chains within the inner part of the bilayered vesicle wall. Such crystalline properties of self-assembled comb-like polymers were also described by Plate and Shibaev, who reported on the tendency for crystallization in the hexagonal crystal structure of polymers with long hydrocarbon side chains [41]. This assumption is further supported with copolymers of shorter hydrophobic block length for which no peak was observed by SAXS (data not shown). The amplitude of the Voigt peak decreases with decreasing concentration (Fig. 4a), indicating the decreasing packing density within the inner bilayer.

The scattering pattern is determined by nanoparticle form-factor only for diluted solutions. However, with the increase of concentration, the interparticle scattering must also be taken into consideration [42]. To account for these interactions in the fitting model, the Percus-Yevik structure factor was applied for concentrations above 1 wt%. In Fig. 4c the structure factors, S(q), for different concentrations of diblock copolymer are shown. The S(q) at small q decreases with increasing concentration from 1 wt% to 5 wt%, indicating increasing repulsive interactions between the particles.

In a subsequent step we evaluated the structural changes in nanoparticles assembled from the fluorinated copolymers. One can see from the Fig. 2a that the SANS scattering curves are rather different from the curves obtained for the diblock copolymer P0 that does not contain a perfluorinated fragment.

For comparison, the SANS and SAXS scattering curves obtained for the polymer with the C_8F_{17} perfluorinated alkyl chain was also fitted by a bilayered vesicle form factor. The final fit and all contributions are shown in Fig. 5a. While the fit of the SAXS data with a bilayered vesicle form factor is quite good, we could not obtain a satisfactory fit of the SANS data. The structural parameters calculated from SANS and SAXS data are presented in Table 2. One can see that the polydispersity over core radius of $PMeOx_{30}$-b-$POctOx_{20}$-C_8F_{17} particles is high, which we explain by the presence of particles of different size and shape. Previous cryo-TEM results [32] indeed revealed the presence of two different species of self-assembled structures, namely bilayered vesicles and worm-like micelles. Therefore, we fitted the scattering curves by a combination of the wormlike micelles form factor and Schultz −Zimm polydispersity radius of a core. It can be seen on Fig. 5(b and d) that the wormlike micelles form factors fit well the scattering curves. Calculated radii of the wormlike micellar core are 8.2 nm from SAXS and 5.2 nm

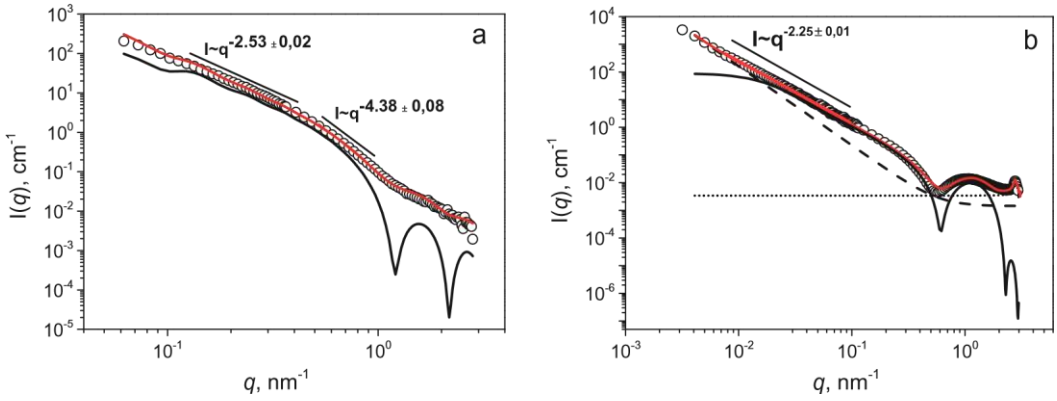

Fig. 3. SANS (a) and SAXS (b) curves of $PMeOx_{30}$-b-$POctOx_{20}$ solutions prepared by direct dissolution. Symbols are experimental scattering data, and red solid lines are fits generated as described in the text. The black solid lines are the form factors of bilayered vesicles, the black dashed lines are the form factors of large aggregates and the black short dotted lines describe the Voigt peak contribution. (For interpretation of the references to colour in this figure legend, the reader is referred to the web version of this article.)

Table 2

Comparison of structural parameters obtained from SAXS and SANS data for $PMeOx_{30}$-b-$POctOx_{20}$ (P0), $PMeOx_{30}$-b-$POctOx_{20}$-C_8F_{17} (P1), $PMeOx_{30}$-b-$POctOx_{20}$-$C_{10}F_{21}$ (P2) and $PMeOx_{30}$-b-$POctOx_{20}$-$C_{12}F_{25}$ (P3). Concentrations are 2wt% for SANS and 2.5 wt% for SAXS.

Fitting parameter	$PMeOx_{30}OctOx_{20}$		$PMeOx_{30}OctOx_{20}$-C_8H_{17}				$PMeOx_{30}OctOx_{20}$-$C_{10}H_{21}$		$PMeOx_{30}OctOx_{20}$-$C_{12}H_{25}$	
	Bilayered vesicle		Bilayered vesicle		Wormlike micelle		Wormlike micelle		Wormlike micelle	
	SAXS	SANS	SAXS	SANS	SAXS	SANS	SAXS	SANS	SAXS	SANS
R_{core} (nm)	25.4	24.4	38.9	16.6	8.2	5.2	9.7	–	2.3	4.9

Sig	0.82	0.26	0.78	0.71	0.12	0.3	–	–	–	–
t_o (nm)	2.2	1.6	5.5	3.0	–	–	–	–	–	–
ti/aVbrush (nm)	2.2	2.5	0.8	1.4	14.4[a]	18.3[a]	15.2[a]		5.6[a]	8.7[a]
Nagg	–	–	–	–	0.12	0.16	0.2		0.19	0.24
xsolv,core	–	–	–	–	0.03	0.01	0.12	–	0.01	0.01
l (nm)	–	–	–	–	4	9.6	4	–	7	7
L (nm)	–	–	–	–	53.0	87.0	65.9	–	72.2	94.0
R_g (nm)	–	–	–	–	5.63	9.0	4.7	–	4.1	3.0
D (nm)	2.27	–	2.27	–	2.29	–	2.3	–	2.0	–
σ	$5 * 10^{-3}$	–	0.14	–	0.14	–	0.22	–	0.2	–
γ	0.1	–	$3 * 10^{-2}$	–	$3 * 10^{-2}$	–	$1.3 * 10^{-3}$	–	0.03	–
α	2.9	2.9	2.7	3	2.8	4	2.7	–	2.6	2.8

R_{core} – core radius, Sig – value of polydispersity, t_o – thickness of outer shell of bilayered vesicle, t_i – thickness of inner shell of bilayered vesicle, V_{core} – volume of a block in a core, V_{brush} – volume of a block in brush, N_{agg} – aggregation number per surface area, $x_{solv,core}$ – amount of solvent in the micellar core, l – Kuhn length, L – contour length, R_g – radius of gyration of the block unit in the corona, D – repeating distance, σ – width of Gaussian profile, γ – width of Lorentzian profile, α – modified Porod exponent.

[a] Shows values that correspond to the second parameter in the row.

from SANS, again in good agreement with the values obtained from cryo-TEM (approximately 7.5 nm) [32]. From the calculated percentage of solvent inside of the wormlike micelles core of 0.03% from SAXS and

0.01 from SANS ($x_{solv,core}$, Table 2), one can assume that the core consists of the highly hydrophobic part of the polymer, probably a mixture of the POctOx and the perfluorinated chains, whereas the outer shell is formed mainly by the hydrophilic PMeOx part. This conclusion is further supported by the fact that the fitted values of the SLD of the micellar core and shell are quite close to the theoretical ones estimated on a basis of their composition. However, the volume of the hydrophilic outer shell and the contour length calculated from the SANS and SAXS curves differs. This can be explained by the discrepancy of the SLD values of the core and the shell determined the octyl chains inside the hydrophobic micellar core as it was mentioned before for the bilayer vesicle structures. Besides, it is known that perfluorinated alkyl chains are quite rigid and also have a tendency to crystallize [43–46]. Based on this we can assume that there are may be two types of ordering inside the nanoparticles. The first one is ordering driven by perfluorinated alkyl chains which form the core of the wormlike micelle. The second one is ordering of the POctOx chains in the first, hydrophobic, shell of the wormlike micelles.

In contrast to the polymer with the shortest perfluorinated fragment, the scattering curves for $PMeOx_{30}$-b-$POctOx_{20}$-$C_{10}F_{21}$ and $PMeOx_{30}$-b-$POctOx_{20}$-$C_{12}F_{25}$ solutions can satisfactorily be fitted with the wormlike micelles form factor only. Scattering and fitting curves with all contributions

by SANS and SAXS as well as by the polydispersity of the system.

The polydispersity may also be explained by the fact that we applied only polydispersity over the core radius of the wormlike micelles that are also polydisperse in their contour length. Probably, the most proper way to fit these data is to combine bilayered vesicle and wormlike micelles form factors with several polydispersities in one fitting procedure, however we are not able to fit such a high number of fitting parameters.

The sharp peak at high q values evidences an additional ordering of

for both polymers are presented in Fig. 6. As for the previous polymers, the final fit of the $PMeOx_{30}$-b-$POctOx_{20}$-$C_{10}F_{21}$ and $PMeOx_{30}$-b-$POctOx_{20}$-$C_{12}F_{25}$ scattering consists of a wormlike micelles form factor with contributions of large aggregates and of a Voigt peak.

The calculated structural parameters are shown in Table 2. The corona volume for the $PMeOx_{30}$-b-$POctOx_{20}$-$C_{10}F_{21}$ wormlike micelles has the highest value. The SLD of the core and the shell of the wormlike micelles formed by $PMeOx_{30}$-b-$POctOx_{20}$-$C_{10}F_{21}$ are almost the same (Table S2), which can mean that the core of micelle contains high

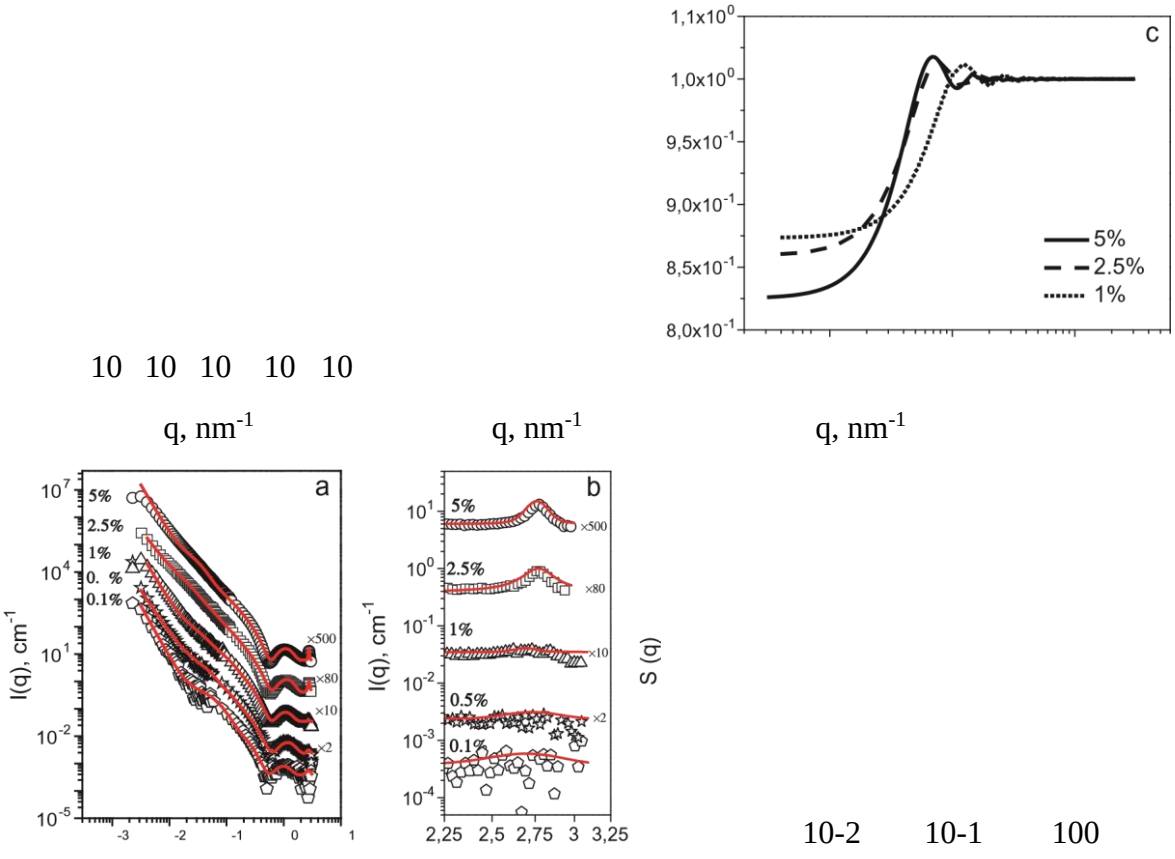

Fig. 4. (a) SAXS data for 0.1, 0.5, 1, 2.5, 5 wt% of $PMeOx_{30}$-b-$POctOx_{20}$ water solutions; (b) 2.25–3.25 nm^{-1} q-range of SAXS data for 0.1, 0.5, 1, 2.5, 5 wt% of $PMeOx_{30}$-b-$POctOx_{20}$ water solutions;

(c) structure factor, S(q), for 1, 2.5, 5% wt% of $PMeOx_{30}$-b-$POctOx_{20}$ water solutions at 25 °C. Symbols are experimental scattering data. Solid lines are fits generated as described in the text.

SANS SAXSFig. 5. SANS (a and b) and SAXS (c and d) curves of

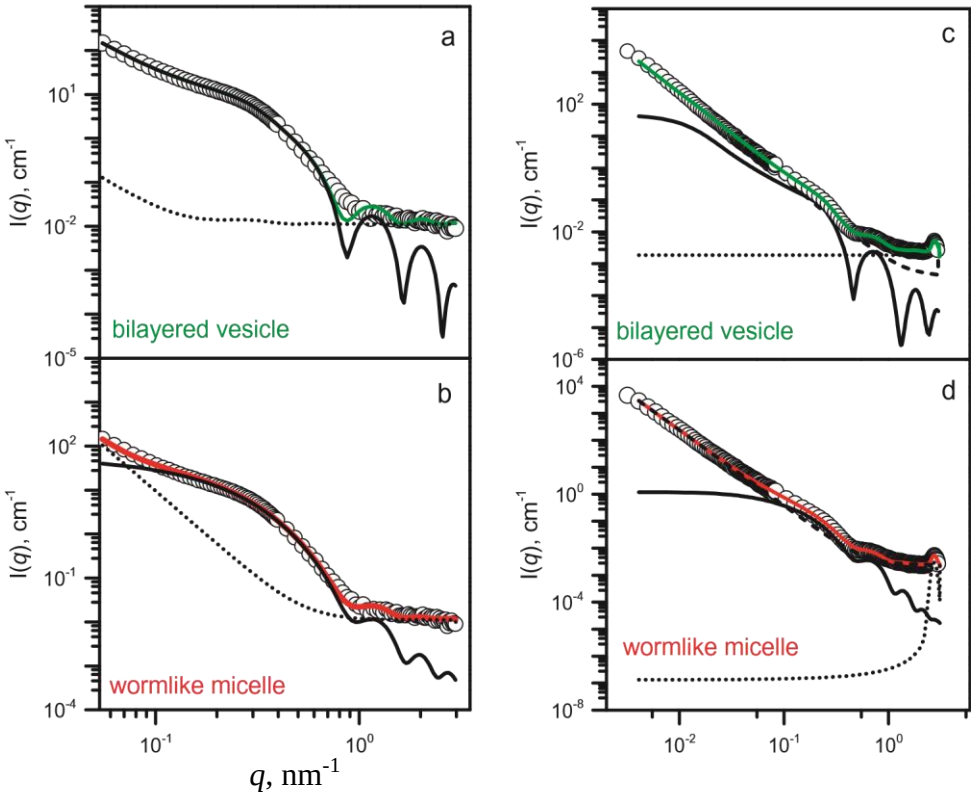

$PMeOx_{30}$-b-$POctOx_{20}$-C_8F_{17} solutions prepared by direct dissolution. Symbols are experimental scattering data. Solid lines are fits generated as described in the text: the bright green solid lines are final fits for bilayered vesicles (a and c), the red lines are final fits of wormlike micelles (b and d). The black solid lines are form factors of individual components: bilayered vesicles (an and c) or wormlike micelles (b and d); black short dashed lines are the form factors of large aggregates and the black short dotted lines correspond to the Voigt peak contribution. (For interpretation of the references to colour in this figure legend, the reader is referred to the web version of this article.)

amount of water and is rather loose. This is further supported by the amount of solvent in the core of 0.12 from SAXS ($x_{solv,core}$, Table 2) resulting from the fitting procedure. Similarly, the contour length of the wormlike micelles formed by $PMeOx_{30}$-b-$POctOx_{20}$-$C_{10}F_{21}$ is shorter compared to the polymer with the highest amount of fluorine: 65.9 nm for $PMeOx_{30}$-b-$POctOx_{20}$-$C_{10}F_{21}$ and 72.2 nm for $PMeOx_{30}$-b-$POctOx_{20}C_{12}F_{25}$. This difference can be explained by the increase in stiffness of the wormlike micelles with increasing perfluorinated chain content.

q, nm^{-1}

Analysis of structural parameters obtained from the fitting procedures (Table 2) gives the possibility to establish the correlation between the length of fluorinated fragment of quasi-triblock poly(2-oxazolines), and morphology of nanoparticles obtained by their self-assembly in water solutions. Dependences of the main parameters on the length of fluorinated fragment in triblock polyoxazolines solutions, prepared by direct dissolution, are presented in Fig. 7.

The obvious changes in morphology are that: (1) the radius of the

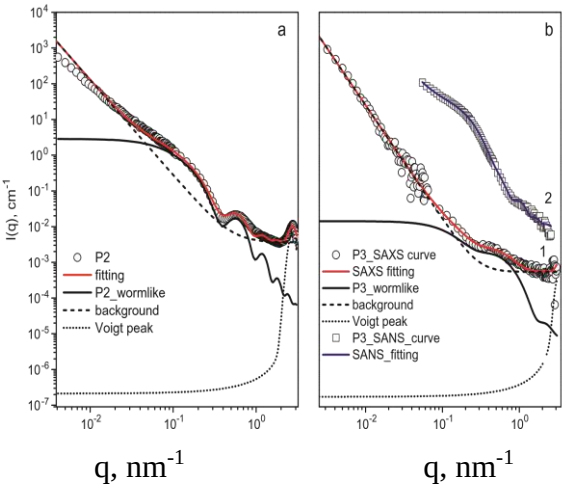

Fig. 6. SAXS (a and b) and SANS (curve no 2 in Fig. 5b) data for $PMeOx_{30}$-b-$POctOx_{20}$-$C_{10}F_{21}$ (P2) and $PMeOx_{30}$-b-$POctOx_{20}$-$C_{12}F_{25}$ (P3) solutions prepared by direct dissolution. Symbols are experimental scattering data. Solid lines are fits generated as described in the text. The black solid lines are form factors of wormlike micelles; black short dashed lines are the form factors of large aggregates and the black short dotted lines are the Voigt peak contributions.

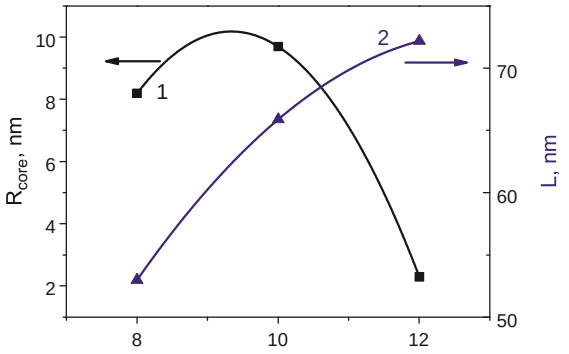

Fig. 7. Dependence of the radius of the wormlike micelles core (1) and contour length of the wormlike micelle (2) as a function of the length of fluorinated fragment in triblock polyoxazolines (solutions prepared by direct dissolution).

wormlike micelles core decrease from 8.2 to 2.3 nm and (2) the contour length of the wormlike micelle increases from 53.0 to 72.2 nm with the increasing of fluorinated fragment length, indicating that wormlike micelles become more long and thin.

4.2. Nanoparticles prepared by solvent exchange method (dialysis)

In a second part of this work, the structures of nanoparticles prepared from the fluorinated quasi-triblock copolymers by solvent exchange (dialysis from methanol against water) are examined. According to the previous DLS results [32], studied polymers present in methanol solutions as individual chains and no self-assembly is observed. In contrast to the results obtained for polymer solutions prepared by direct dissolution method, DLS and cryo-TEM studies of aqueous solution of quasi-triblock copolymers prepared by solvent exchange method revealed the presence of spherical micelles with diameter 15–20 nm.

The obtained scattering curves are quite similar for all polymer water solutions (Fig. 8). There is no sign of aggregation of the selfassembled structures. For all obtained aqueous polymer solutions, the formed nanoparticles revealed a core–shell structure consisting of one or two layers with spherical symmetry. To fit the scattering data a model of sphere with two shells has, thus, been chosen.

Despite the fact that the diblock copolymer consists of two blocks, which can form a core with just one shell, the model of sphere with one shell did not fit correctly the scattering curve. We assume that the presence of a second shell (calculated from the fitting procedure) can be related to the inhomogeneously distributed density of the hydrophobic and hydrophilic parts of the micelle and that the indistinct border between the core and the shell can affect the values of the SLD. From the

Table 3
Comparison of structural parameters obtained from all samples $PMeOx_{30}$-b-$POctOx_{20}$ (P0), $PMeOx_{30}$-b-$POctOx_{20}$-C_8F_{17} (P1), $PMeOx_{30}$-b-$POctOx_{20}$-$C_{10}F_{21}$ (P2) and $PMeOx_{30}$-b$POctOx_{20}$-$C_{12}F_{25}$ (P3) prepared by solvent exchange by SAXS.

Fitting parameter	PMeOx$_{30}$-b-POctOx$_{20}$	PMeOx-b-POctOx-C$_8$F$_{17}$	PMeOx-b-POctOx-C10F21	PMeOx-b-POctOx-C12F25
R_{core} (nm)	5.19	4.72	3.7	3.76
sig	0.21	0.17	0.58	0.04
t_1	3.06	2.49	9.9	7.08
t_2	6.96	6.47	3.89	5.61
D (nm)	2.22	2.22	2.26	
σ	0.086	0.115	0.078	0.12
γ	0.1	0.145	0.108	0.09
α	1	1	1	1.13

R_{core} – core radius, Sig – value of polydispersity, t_1 – thickness of first shell of sphere, t_2 – thickness of second shell of sphere, D – repeat distance, σ– width of Gaussian (Doppler) profile, γ – width of Lorentzian profile, α – modified Porod exponent.

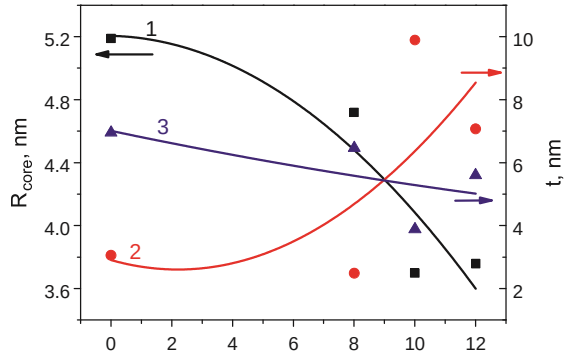

Fig. 9. Dependence of the core radius (R_{core}) (1), thickness (t) of the first (2) and second (3) shell on the length of fluorinated fragment of triblock polyoxazoline polymers (solutions prepared by solvent exchange method).

position of the first minimum in the scattering curve, the radius of a sphere (R) with core-double shell structure could be determined to be approximately 15.2 nm using the following equation qR =4.493 [47].

It is obvious from Fig. 8b that the intensity of the peak at high q values decreases with increasing length of the fluorinated block. This feature may be related to the presence of two types of water-insoluble chains that both have a tendency to crystallize. While the POctOx segments form more strictly ordered structures due to the conditional homogeneity inside the core, the presence of fluorinated units penalize the homogeneity of the core and of one of the shells, thus reducing the ordering.

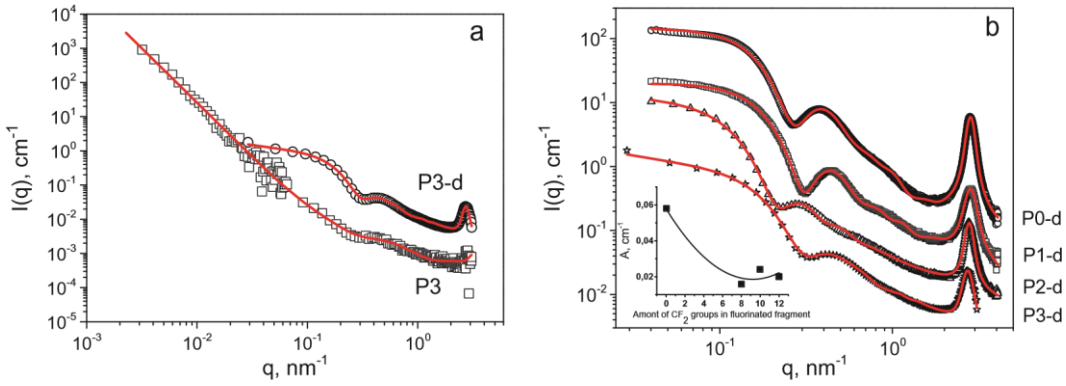

Fig. 8. (a) Comparison of SAXS data for $PMeOx_{30}$-b-$POctOx_{20}$-$C_{12}F_{25}$ (P3) prepared by direct dissolution and by solvent exchange; (b) Comparison of SAXS data for all polymers prepared by solvent exchange and (b inset) dependence of maximum amplitude of Voigt peak (calculated by fitting procedure) on the length of fluorinated fragment for nanoparticles prepared by solvent exchange method.

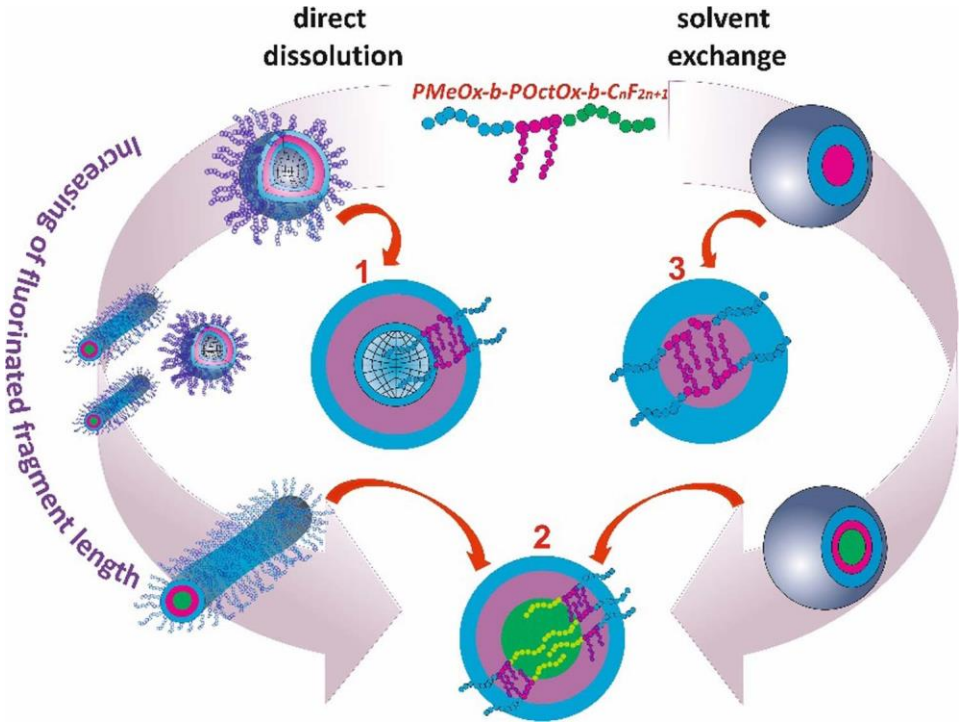

Fig. 10. A proposed scheme of morphological transition of the fluorinated $PMeOx_{30}$-b-$POctOx_{20}$-C_nF_{2n+1} nanoparticles (prepared by direct dissolution and by solvent exchange method) with increasing length of fluorinated fragment summarizing the SAXS and SANS results, where: 1 – scheme of the inner structure of bilayered vesicle formed by $PMeOx_{30}$-b-$POctOx_{20}$ and $PMeOx_{30}$-b-$POctOx_{20}$-$C_{10}F_{21}$; 2 – scheme of the inner structure of wormlike micelle and core-shellshell sphere formed by $PMeOx_{30}$-b-$POctOx_{20}C_nF_{2n+1}$; 3 – scheme of the sphere with core-shell inner structure.

Dependences of the main structural parameters (Table 3) obtained from the fitting procedure on the length of fluorinated fragment are presented in the Fig. 9.

One can see that the thickness of the second shell, consist of poly(2methyl-2-oxazoline) block, varies only slightly, while thickness of the first shell increase with the increasing of the length of fluorinated fragment. At the same time core radius decreases with the increasing of the fluorinated part length. It can be explained by the assumption that for copolymer PMeOx30-b-POctOx20-C_8F_{17} with the shortest fluorinated fragment poly(2-octyl-2-oxazoline) block is more hydrophobic then fluorinated part. That

is why the core the sphere for PMeOx30-bPOctOx20-C_8F_{17} consists of the poly(2-octyl-2-oxazoline) block as it was for diblock copolymer. With increasing of the length of fluorinated fragment its hydrophobicity increase and for PMeOx30-b-POctOx20-
$C_{10}F_{21}$ and PMeOx30-b-POctOx20-$C_{12}F_{25}$ the core is formed mainly by fluorinated groups. We can also assume that the first hydrophobic shell consist of poly(2-octyl-2-oxazoline) block with partially involved fluorinated fragment.

The proposed scheme of morphological transition observed in this study is presented in the Fig. 10. It can be concluded from the comparison of the SAXS and SANS results as well as of DLS and cryo-TEM results presented recently [32] that shape and inner structure of fluorinated quasi-triblock poly(2-oxazolines) can be easily controlled by the changing of terminal fluorinated group as well as by the method of preparation.

5. Conclusions

Aqueous self-assembly of quasi-triblock copolymers composed of hydrophilic, hydrophobic and perfluorinated blocks was studied at room temperature using SAXS and SANS analysis. Detailed information about the shape and the internal structure of the self-assembled nanoparticles as function of their composition and fluorine content was obtained and compared with previously obtained cryo-TEM data. Nanoparticles formed by the reference diblock $PMeOx_{30}$-b-$POctOx_{20}$ without fluorinated segment could be described by a bilayered vesicle form factor in combination with a Percus-Yevick structure factor. SANS and SAXS experiments revealed the morphological transition of micelles from bilayered vesicles to wormlike micelles with increasing length of the perfluorinated fragment of the quasi-triblock PAOx. It was further found that the preparation method influences the nanoparticles' shape and internal structure: with solvent displacement it becomes independent of the fluorine content and the SAXS curves could be fitted with a core–shell-shell form factor. Additional ordering was identified within the inner layer of bilayered vesicles, core of wormlike micelles as well as inside of the core of spheres, probably due to the crystallization of the POctOx and perfluorinated segments, and was described with a Voigt peak model.

Acknowledgments

Sergey K. Filippov and Richard Hoogenboom acknowledge the support of the mobility project AV ČR – FWO FWO-17-05. Sergey K. Filippov acknowledges financial support of Ministry of Education, Youth and Sports of the Czech Republic, grant No. LH15213. ESRF (Grenoble, France), LLB (Saclay, France), and Diamond Light Source (Didcot, UK) are acknowledged for beam time allocation. We also acknowledge HZB for allocation of neutron beamtime. This work was also supported by the Ministry of Education, Youth and Sports of CR within the National Sustainability Program I (Project POLYMAT LO1507).

Notes

The authors declare no competing financial interest.

Appendix A. Supplementary material

Supplementary data associated with this article can be found, in the online version, at http://dx.doi.org/10.1016/j.eurpolymj.2018.01.007.

References

[1] T.X. Viegas, M.D. Bentley, J.M. Harris, Z. Fang, K. Yoon, B. Dizman, R. Weimer, A. Mero, G. Pasut, F.M. Veronese, Polyoxazoline: chemistry, properties, and applications in drug delivery, Bioconjug. Chem. 22 (5) (2011) 976–986.

[2] M.C. Woodle, C.M. Engbers, S. Zalipsky, New amphipatic polymer-lipid conjugates forming long-circulating reticuloendothelial system-evading liposomes, Bioconjug. Chem. 5 (1994) 493–496.

[3] M. Hrubý, S.K. Filippov, P. Štěpánek, Smart polymers in drug delivery systems on crossroads: which way deserves following? Eur. Polym. J. 65 (2015) 82–97.

[4] R. Luxenhofer, Y. Han, A. Schulz, J. Tong, Z. He, A.V. Kabanov, R. Jordan, Poly (2oxazoline)s as polymer therapeutics, Macromol. Rapid Commun. 33 (2012) 1613–1631.

[5] B. Guillerm, V. Darcos, V. Lapinte, S. Monge, J. Coudane, J.-J. Robin, Synthesis and evaluation of triazole-linked poly(ε-caprolactone)-graft-poly(2-methyl-2-oxazoline) copolymers as potential drug carriers, Chem. Commun. 48 (2012) 2879–2881.

[6] M. Hruby, S.K. Filippov, J. Panek, M. Novakova, H. Mackova, J. Kucka, D. Vetvicka, K. Ulbrich, Polyoxazoline thermoresponsive micelles as radionuclide delivery systems, Macromol. Biosci. 10 (2010) 916–924.

[7] G.-H. Hsiue, H.-Z. Chiang, C.-H. Wang, T.-M. Juang, Nonviral gene carriers based on diblock copolymers of poly(2-ethyl-2-oxazoline) and linear polyethylenimine, Bioconjug. Chem. 17 (2006) 781–786.

[8] B. Pidhatika, M. Rodenstein, Y. Chen, E. Rakhmatullina, A. Muhlebach, C. Acikguz, M. Textor, R. Konradi, Comparative stability studies of poly(2-methyl-2-oxazoline) and poly(ethylene glycol) brush coatings, Biointerphases 7 (2012) 1–4.

[9] D.A. Tomalia, D.P. Sheetz, Homopolymerization of 2-alkyl- and 2-aryl-2-oxazolines, J. Polym. Sci. Part A-1 Polym. Chem. 4 (1966) 2253–2265.

[10] B. Verbraeken, B.D. Monnery, K. Lava, R. Hoogenboom, The Chemistry of poly(2oxazoline)s, Eur. Polym. J. (2016).

[11] M.A. Tasdelen, M.U. Kahveci, Y. Yagci, Telechelic polymers by living and controlled/living polymerization methods, Prog. Polym. Sci. 36 (2011) 455–567.

[12] B. Guillerm, S. Monge, V. Lapinte, J.J. Robin, How to modulate the chemical structure of polyoxazolines by appropriate functionalization, Macromol. Rapid Commun. 33 (2012) 1600–1612.

[13] K. Lava, B. Verbraeken, R. Hoogenboom, Poly(2-Oxazoline)s and click chemistry: a versatile toolbox toward multi-functional polymers, Eur. Polym. J. 65 (2015) 98–111.

[14] B. Trzebicka, N. Koseva, V. Mitova, A. Dworak, Organization of poly(2-ethyl-2oxazoline)-block-poly(2-phenyl-2-oxazoline) copolymers in water solution, Polymer (Guildf) 51 (2010) 2486–2493.

[15] J. Du, Polymer vesicles, Adv. Hierarchical Nanostruct. Mater. 967 (2002) 177–192.
[16] S. Zalipsky, C.B. Hansen, J.M. Oaks, T.M. Allen, Evaluation of blood clearance rates and biodistribution of poly(2-oxazoline)-grafted liposomes, J. Pharm. Sci. 85 (1996) 133–137.
[17] Y. Milonaki, E. Kaditi, S. Pispas, C. Demetzos, Amphiphilic gradient copolymers of 2-methyl- and 2-phenyl-2-oxazoline: self-organization in aqueous media and drug encapsulation, J. Polym. Sci. Part A Polym. Chem. 50 (2012) 1226–1237.
[18] R. Luxenhofer, A. Schulz, C. Roques, S. Li, T.K. Bronich, E.V. Batrakova, R. Jordan, A.V. Kabanov, Doubly amphiphilic poly(2-oxazoline)s as high-capacity delivery systems for hydrophobic drugs, Biomaterials 31 (2010) 4972–4979.
[19] A.O. Moughton, M.A. Hillmyer, T.P. Lodge, Multicompartment block polymer micelles, Macromolecules 45 (2012) 2–19.
[20] Z. Li, E. Kesselman, Y. Talmon, M.A. Hillmyer, T.P. Lodge, Multicompartment micelles from ABC Miktoarm stars in water, Science 306 (5693) (2004) 98–110. [21] S. Kubowicz, J.F. Baussard, J.F. Lutz, A.F. Thünemann, H. Von Berlepsch, A. Laschewsky, Multicompartment micelles formed by self-assembly of linear ABC triblock copolymers in aqueous medium, Angew. Chemie - Int. Ed. 44 (33) (2005) 5262–5265.
[22] F. Tournilhac, L. Bosio, J.F. Nicoud, J. Simon, Polyphilic molecules: synthesis and mesomorphic properties of a four-block molecule, Chem. Phys. Lett. 145 (5) (1988) 452–454.
[23] L. Campo, T. Varslot, M.J. Moghaddam, J.J.K. Kirkensgaard, K. Mortensen, S.T. Hyde, A novel lyotropic liquid crystal formed by triphilic star-polyphiles: hydrophilic/oleophilic/fluorophilic rods arranged in a 12.6.4. tiling, Phys. Chem.
Chem. Phys. 13 (2011) 3139–3152.
[24] S.T. Hyde, L. de Campo, C. Oguey, Tricontinuous mesophases of balanced three-arm “star Polyphiles”, Soft Matter 5 (2009) 2782.
[25] G.F. von Rudorff, T. Watermann, X.-Y. Guo, D. Sebastiani, Conformational space of a polyphilic molecule with a fluorophilic side chain integrated in a DPPC bilayer, J.
Comput. Chem. 38 (9) (2017) 576–583.
[26] D.J. Pochan, Z. Chen, H. Cui, K. Hales, K. Qi, K.L. Wooley, Toroidal triblock copolymer assemblies, Science 306 (5693) (2004) 94–97.
[27] K. Kempe, R. Hoogenboom, S. Hoeppener, C.-A. Fustin, J.-F. Gohy, U.S. Schubert, Discovering new block terpolymer micellar morphologies, Chem. Commun.
(Camb). 46 (35) (2010) 6455–6457.
[28] H. Peng, I. Blakey, B. Dargaville, F. Rasoul, S. Rose, A.K. Whittaker, Synthesis and evaluation of partly fluorinated block copolymers as MRI imaging agents, Biomacromolecules 10 (2009) 374–381.
[29] K. Wang, H. Peng, K.J. Thurecht, S. Puttick, A.K. Whittaker, PH-responsive star polymer nanoparticles: potential 19F MRI contrast agents for tumour-selective imaging, Polym. Chem. 4 (16) (2013) 4480–4489.
[30] U. Mansfeld, S. Hoeppener, K. Kempe, J.-M. Schumers, J.-F. Gohy, U.S. Schubert, Tuning the morphology of triblock terpoly(2-oxazoline)s containing a 2-phenyl-2oxazoline block with varying fluorine content, Soft Matter 9 (25) (2013) 5966.

[31] R. Weberskirch, J. Preuschen, H.W. Spiess, O. Nuyken, Design and synthesis of a two compartment micellar system based on the self-association behavior of poly(Nacylethyleneimine) end-capped with a fluorocarbon and a hydrocarbon chain, Macromol. Chem. Phys. 201 (10) (2000) 995–1007.

[32] L.I. Kaberov, B. Verbraeken, M. Hruby, A. Riabtseva, L. Kovacik, S. Kereïche, J. Brus, P. Stepanek, R. Hoogenboom, S.K. Filippov, Novel triphilic block copolymers based on poly(2-methyl-2-oxazoline)–block–poly(2-octyl-2-oxazoline) with different terminal perfluoroalkyl fragments: synthesis and self-assembly behaviour, Eur. Polym. J. 88 (2017) 645–655.

[33] I. Bressler, J. Kohlbrecher, A.F. Thanemann, SASfit: a tool for small-angle scattering data analysis using a library of analytical expressions, J. Appl. Crystallogr. 48 (2015) 1587–1598.

[34] J.K. Percus, G.J. Yevick, Analysis of classical statistical mechanics by means of collective coordinates, Phys. Rev. 110 (1958) 1–13.

[35] J.S. Pedersen, M.C. Gerstenberg, Scattering form factor of block copolymer micelles, Macromolecules 29 (1996) 1363–1365.

[36] A.L. Kholodenko, Analytical calculation of the scattering function for polymers of arbitrary flexibility using the dirac propagator, Macromolecules 26 (1993) 4179–4183.

[37] A. Guinier, G. Fournet, G. Fournet (Ed.), Small-Angle Scattering of X-Rays, John Wiley and Sons, New York, 1955.

[38] M.J. Derry, O.O. Mykhaylyk, S.P. Armes, A vesicle-to-worm transition provides a new high-temperature oil thickening mechanism, Angew. Chemie - Int. Ed. 56 (7) (2017) 1746–1750.

[39] N. Baccile, A.S. Cuvier, S. Provost, C.V. Stevens, E. Delbeke, J. Berton, W. Soetaert, I.N.A. Van Bogaert, S. Roelants, Self-assembly mechanism of pH-responsive glycolipids: micelles, fibers, vesicles, and bilayers, Langmuir 32 (2016) 10881–10894.

[40] D. Balzar, H. Ledbetter, Voigt-function modeling in fourier analysis of size- and strain-broadened X-ray diffraction peaks, J. Appl. Crystallogr. 26 (pt 1) (1993) 97–103.

[41] N.A. Plate, V.P. Shibaev, Comb-Shaped Polymers and Liquid Crystals, Plenum Press, New York, 1987.

[42] B. Weyerich, J. Brunner-Popela, O. Glatter, Small-angle scattering of interacting particles. II. Generalized indirect fourier transformation under consideration of the effective structure factor for polydisperse systems, J. Appl. Crystallogr. 32 (1999) 197–209.

[43] L.M. Wilson, A.C. Griffin, Liquid crystalline fluorocarbon side-chain polyesters, Macromolecules 27 (1994) 1928–1931.

[44] L.M. Wilson, A.C. Griffin, Liquid-crystalline behavior in a series of fluorocarbon side-chain polyesters. 2, Macromolecules 27 (1994) 4611–4614.

[45] A. Hirao, G. Koide, K. Sugiyama, Synthesis of novel well-defined chain-end- and inchain-functionalized polystyrenes with one, two, three, and four perfluorooctyl groups and their surface characterization, Macromolecules 35 (2002) 7642–7651. [46] V.V. Volkov, N.A. Plate, A. Takahara, T. Kajiyama, N. Amaya, Y. Murata, Aggregation state and mesophase structure of comb-shaped polymers with fluorocarbon side groups, Polymer (Guildf). 33 (1992) 1316–1320.

[47] O. Glatter, O. Kratky, Small-angle X-ray scattering, Academic Press, London, 1982.